Giant Vesicles under Oxidative Stress Induced by a Membrane-Anchored Photosensitizer

Karin A. Riske,[†]* Tatiane P. Sudbrack,[‡] Nathaly L. Archilha,[‡] Adjaci F. Uchoa,[§] André P. Schroder,[¶]
Carlos M. Marques,[¶] Maurício S. Baptista,[§] and Rosangela Itri[‡]
[†]Departamento de Biofísica, Universidade Federal de São Paulo, São Paulo, Brazil; [‡]Departamento de Física Aplicada, Instituto de Física, [§]Departamento de Bioquímica, Instituto de Química, Universidade de São Paulo, São Paulo, Brazil; and [¶]Institut Charles Sadron, Université de Strasbourg, Centre National de la Recherche Scientifique, Strasbourg, France

ABSTRACT　We have synthesized the amphiphile photosensitizer PE-porph consisting of a porphyrin bound to a lipid head-group. We studied by optical microscopy the response to light irradiation of giant unilamellar vesicles of mixtures of unsaturated phosphatidylcholine lipids and PE-porph. In this configuration, singlet oxygen is produced at the bilayer surface by the anchored porphyrin. Under irradiation, the PE-porph decorated giant unilamellar vesicles exhibit a rapid increase in surface area with concomitant morphological changes. We quantify the surface area increase of the bilayers as a function of time and photosensitizer molar fraction. We attribute this expansion to hydroperoxide formation by the reaction of the singlet oxygen with the unsaturated bonds. Considering data from numeric simulations of relative area increase per phospholipid oxidized (15%), we measure the efficiency of the oxidative reactions. We conclude that for every 270 singlet oxygen molecules produced by the layer of anchored porphyrins, one eventually reacts to generate a hydroperoxide species. Remarkably, the integrity of the membrane is preserved in the full experimental range explored here, up to a hydroperoxide content of 60%, inducing an 8% relative area expansion.

INTRODUCTION

It is well known that biological membranes contain a large amount of unsaturated lipids, which are susceptible to the attack of singlet oxygen and free radicals. These reactions generate lipid hydroperoxides and a large variety of unstable lipid species, which can lead to extensive free radical chain reactions. Oxidative stress can cause severe membrane damage and even cell death; although it is not yet clear to what extent the formation of lipid hydroperoxides is directly responsible for cell damaging. Peroxidation of lipids has been widely studied both in biological membrane extracts and in model lipid bilayers, and involves several reactions that depend both on membrane properties and on the oxidative agent (see (1) for a review). Oxidative reactions alter the chemical structure of unsaturated lipids, leading to changes in lipid bilayer properties, such as permeability, fluidity, and packing order (1–6). Though less emphasized, lipid peroxidation firstly causes an increase in area per lipid (2,5). Molecular dynamics simulations have shown (5) that the hydroperoxide group has a tendency to reside close to the bilayer surface, due to its more hydrophilic character, resulting in an increase in area per lipid. Such area increase upon oxidation has been reported on lipid monolayers (7–9), but it has never been experimentally quantified in lipid bilayers.

Oxidative processes can be therapeutically used to kill tumor cells and heal several skin diseases. Photodynamic therapy (10) consists of directing a photosensitive molecule to a target tissue, e.g., tumors, followed by irradiation with light. Photosensitive molecules, such as porphyrin derivatives or methylene blue, can easily transfer their energy to molecular oxygen thus generating singlet oxygen $^1O_2$ and/or free radicals. When irradiated, photosensitive molecules trigger oxidative reactions in the targeting tissue, causing oxidation of several biomolecules, which eventually lead to cell apoptosis/necrosis. Though final tissue death is a complex process that involves several intermediate steps, it is believed that damaging membranes is one of the first and key steps (11,12). Some literature data also suggest that membrane proteins may be the main triggers of processes leading to cell death (13). Even so, the reaction efficiency between singlet oxygen and unsaturated lipids, as well as the relationship between the extent of lipid peroxidation and the corresponding changes in the physical properties of membranes, are not yet known.

The effects of oxidative stress on model lipid membranes can be addressed by optical observation of giant unilamellar vesicles (GUVs). GUVs have diameters of ~10 μm, similar to cells, and allow for optical observation in real-time, which make them a handy tool to study different aspects of lipid bilayers (14,15). Damage to membranes due to photoactivation of methylene blue present in the surrounding solution was previously studied by optical microscopy of GUVs made of dioleoyl phosphatidylcholine (16). GUVs immersed in a micromolar solution of methylene blue were destroyed upon few minutes of irradiation. The mechanism of membrane damage was attributed to lipid chain break with formation of short-chain amphiphiles (16).

In this work, we investigate photoinduced effects of a new porphyrin derivative incorporated in GUVs of palmitoyl

oleoyl phosphatidylcholine (POPC). This new photosensitive molecule, PE-porph, was synthesized by us and consists of a porphyrin molecule chemically linked to the headgroup of two phosphatidylethanolamines (PE) (Fig. 1 A). The key advantage of PE-porph is that it inserts into the bilayer, and therefore the photosensitive group is anchored on the bilayer. This localization ensures that the production of $^1O_2$ occurs close to its main target, the acyl chain double-bond of POPC.

We report here that irradiation of the anchored PE-porph induces morphological changes of GUVs, driven by an increase in surface area induced by lipid peroxidation. The increase in area is here quantified, taking advantage of the fact that lipid vesicles assume prolate shapes when subjected to an alternating current (AC) field (17). Since at constant field strength the magnitude of vesicle elongation depends on the excess area of the particular vesicle, we were able to monitor the membrane area increase as a function of the irradiation time for several different molar fractions of PE-porph. The comparison between the amount of singlet oxygen generated by PE-porph and the corresponding production of lipid hydroperoxides allowed us to estimate the efficiency of reaction between singlet oxygen and unsaturated lipids.

MATERIALS AND METHODS

Materials

The phospholipids 1-palmitoyl-2-oleoyl-sn-glycero-3-phosphocholine (POPC) and 1,2-dimyristoyl-sn-glycero-3-phosphoethanolamine (DMPE)

were purchased from Avanti Polar Lipids (Alabaster, AL). The photosensitizer dimethyl 8,13-divinyl-3,7,12,17-tetramethyl-21H,23H-porphine-2,-18-dipropyl-L-α-dimyristoylphosphatidylethanolamine (PE-porph) was synthesized as described below.

PE-porph synthesis

PE-porph was obtained by the addition of dimyristoyl phosphatidylethanolamine (DMPE) to acyl chloride of protoporphyrin IX ($\geq$95%, purchased from Sigma-Aldrich, St. Louis, MO), both in previously dried dichloromethane. The solvent excess was removed by reduced pressure and PE-porph was purified by column chromatography, using silica gel 230:70 as stationary phase eluate with $CHCl_2$/MeOH 20:1. The reaction occurred with a final yield of 71%. The product formation was initially characterized in thin layer chromatography showing a single spot with radio frequency of 0.65 in $CHCl_2$/MeOH 20:1. Ultraviolet visible (UV-VIS) spectroscopy and fluorescence spectra show the same features as the original chromophore, therefore the reaction occurred without changes in the porphyrin ring (Fig. 1 B). The infrared spectrum shows a broad and intense band at 3400 cm^{-1}, due to the axial OH deformation; two bands at 2922 and 2852 cm^{-1}, characteristic of axial CH, CH_2, and CH_3 deformations present in the alkyl chains of phosphatidylethanolamine; and an intense band at 1735 cm^{-1} due to the axial C=O deformation, which is characteristic of amides derived from protoporphyrin IX. In the mass spectrum, the mass peak of the ion molecular (1799 m/z) is within the detection limit. However, the pattern of fragmentation along with the data from infrared and UV-VIS spectroscopy allowed the unequivocal determination of the structure of PE-porph. Several signals with high mass prove the functionalization with the phospholipid molecule. The presence of peaks every 14 units are characteristic of molecules with high-molecular-weight alkyl chains. Furthermore, the peak at 569.3 m/z can be associated to N/OC rupture of one of the amides and chain break at the second amide (Porphyrin-NCH_2CH_2/OPO_3R). Another peak at 1115.7 m/z was attributed to the fragment $C_{55}H_{79}N_6O_{10}P$, resulting from oxygen-phosphorus break
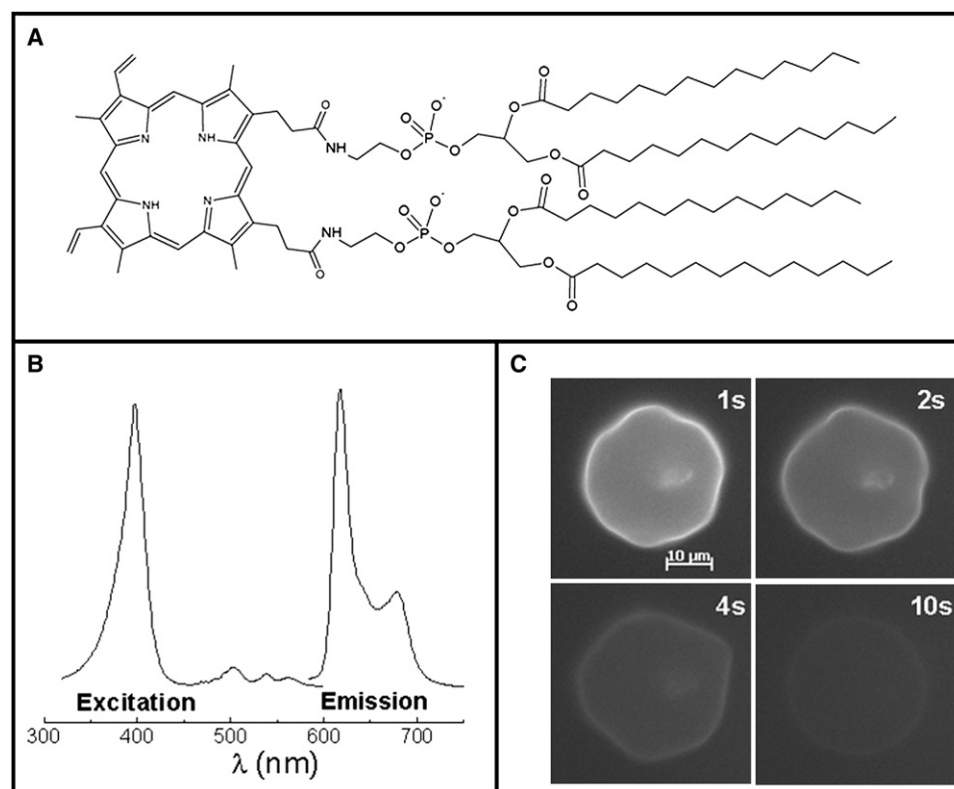

FIGURE 1 Characteristics of the photosensitive molecule PE-porph. (A) Chemical structure. (B) Excitation and emission spectra of POPC GUVs with $X_{porph} = 0.05$. (C) Fluorescence microscopy images of a POPC GUV containing $X_{porph} = 0.03$ as a function of the irradiation time shown on the top of each snapshot. The scale bar represents 10 μm.

(PpIX-NCH$_2$CH$_2$O/PO$_3$R1) of one of the PEs, and ester hydrolysis in one of the tails of the second PE group.

Preparation of giant unilamellar vesicles

Giant unilamellar vesicles of POPC containing different molar fractions of PE-porph ($X_{porph} = 0.005$–0.1, i.e., 0.5–10 mol %) were grown using the electroformation method (18). Briefly, 16 μL of a 2 mg/mL lipid/PE-porph chloroform solution were spread on the surfaces of two conductive glasses (coated with Fluor Tin Oxide), which were then placed with their conductive sides facing each other and separated by a 2-mm-thick Teflon frame. This electroswelling chamber was filled with 0.2 M sucrose solution and connected to an alternating power generator at 1 V with a 10 Hz frequency for 1–2 h. The vesicle solution was removed from the chamber and diluted ~10 times into a 0.2 M glucose solution. This created a sugar asymmetry between the interior and the exterior of the vesicles. The osmolarities of the sucrose and glucose solutions were measured with a cryoscopic osmometer Osmomat 030 (Gonotec, Berlin, Germany) and carefully matched to avoid osmotic pressure effects. The vesicle solution was placed in an observation chamber. Due to the differences in density and refractive index between the sucrose and glucose solutions, the vesicles were stabilized by gravity at the bottom of the chamber and had better contrast when observed with phase contrast microscopy.

Optical microscopy observation and irradiation

Observation of giant vesicles was performed under an inverted microscope, Axiovert 200 (Carl Zeiss, Jena, Germany), equipped with a Ph2 63× objective. Images were taken with an AxioCam HSm digital camera (Carl Zeiss). Irradiation of the samples was performed using the HBO 103W Hg lamp of the microscope using a 400-nm excitation filter. The power density of the irradiation was 5 W/cm^2, measured with a Powermeter (Coherent, Santa Clara, CA). Some experiments were performed in the presence of an alternating electrical (AC) field of 10 V intensity and 1 MHz frequency. In those cases, the vesicles contained a small amount of salt (0.5 mM NaCl) to ensure a higher conductivity inside, and thus to induce prolate deformation (17). For these measurements, the vesicle solution was placed in a special chamber purchased from Eppendorf (Hamburg, Germany), which consists of an 8-mm-thick Teflon frame confined between two glass plates through which observation was possible. A pair of parallel platinum electrode wires with 90 μm in radius was fixed at the lower glass. The gap distance between the two wires was 0.5 mm. The chamber was connected to a function generator.

PE-porph incorporated in POPC dispersions: absorption and fluorescence spectra and singlet oxygen production

Some control experiments were done with $X_{porph} = 0.05$ in 0.1 mM POPC dispersions (prepared by vortex, yielding multilamellar vesicles). Absorbance spectra were recorded on a UV-VIS 2400-PC spectrophotometer (Shimadzu, Kyoto, Japan). Fluorescence spectra were recorded in a Fluorog (Spex, Lisbon, Portugal) in right-angle mode interfaced to a PC, controlled by DM3000-F software. Absorbance at 400 nm and fluorescence emission at 640 nm (excitation at 400 nm) were followed as a function of irradiation time with a conventional laser ($\lambda = 532$ nm, 5 mW), and were found to decrease ~15% after 25 min irradiation. The singlet oxygen $^1O_2$ production was determined by using a phosphorescence detection method. A pulsed Surelite III Nd:YAG laser (Continuum, West Newton, MA) was used as the excitation source operating at 532 nm (5 ns, 10 Hz). The radiation emitted at 1270 nm was detected at right angle by a liquid nitrogen-cooled photomultiplier, model No. R5509 (Hamamatsu, Hamamatsu City, Japan) (19). The quantum yield of $^1O_2$ production, Φ_Δ, was calculated by measuring and comparing the emissions of sample (PE-porph) and standard (Hematoporphyrin IX), whose Φ_Δ is 0.76 (20). Sample and standard solutions were prepared in methanol and absorptions were matched and amounted to 0.20 at 532 nm.

RESULTS

Characterization of the photosensitive molecule PE-porph

The photosensitive molecule synthesized consists of a porphyrin molecule attached to two phosphatidylethanolamines, as schematically shown in Fig. 1 A. The main spectral characteristics of PE-porph are quite similar to those observed for porphyrin incorporated in model membranes (21,22), with the maximum absorption at ~400 nm and the emission above 600 nm (see Fig. 1 B). The quantum yield of singlet oxygen ($^1O_2$) production, Φ_Δ, was determined to be equal to 0.50. Observation under the microscope in the fluorescence mode showed that the porphyrin is incorporated in the bilayer, as shown in Fig. 1 C for a GUV containing 3 mol % of PE-porph. After some exposure to the excitation light, photobleaching of PE-porph occurred. Under our strongest illumination conditions, i.e., full power of the Hg lamp, photobleaching occurred typically within seconds, as can be seen in the sequence of fluorescence snapshots shown in Fig. 1 C.

Morphological changes of GUVs caused by irradiation of PE-porph

Giant unilamellar vesicles (GUVs) of POPC containing $X_{porph} = 0.005$–0.1 (0.5–10 mol % PE-porph) were irradiated and simultaneously observed under an optical microscope. Visible morphological shape changes occurred in the GUVs as soon as the irradiation started. Some examples are shown in Fig. 2 for vesicles with $X_{porph} = 0.02$ and 0.05. All vesicles showed an increase in their projected area. The increase in projected area was often accompanied by an increase in thermal fluctuations, especially when vesicles were initially spherical and tense; see the first snapshots in Fig. 2, A and B. This is a clear indication that the area-to-volume ratio increased during illumination. At low PE-porph molar fraction (see Fig. 2 A), the increase in excess area was moderate, resulting mainly in an increase of the apparent vesicle diameter. One can also discern a small increase in the shape roughness in the last snapshot of the figure. At higher PE-porph molar fractions, the increase in excess area and shape fluctuations appeared clearly (see Fig. 2 B). During the process, the vesicles generally became flatter, such that the focal plane of the vesicle equator was shifted to a lower level; see, for instance, the snapshot at 5 s in Fig. 2 A. In many cases, vesicles containing more than $X_{porph} = 0.02$ expelled some buds, i.e., satellite vesicles still connected to the mother vesicle through thin necks; see snapshot at 43 s in Fig. 2 C. The initial sugar asymmetry, seen by the presence of the phase contrast rings, was roughly maintained throughout the irradiation process, showing that no significant change in bilayer permeability has occurred, e.g., there was no opening of pores. We argue in the following that the morphological changes described above, i.e., the increase in projected area and in fluctuations,
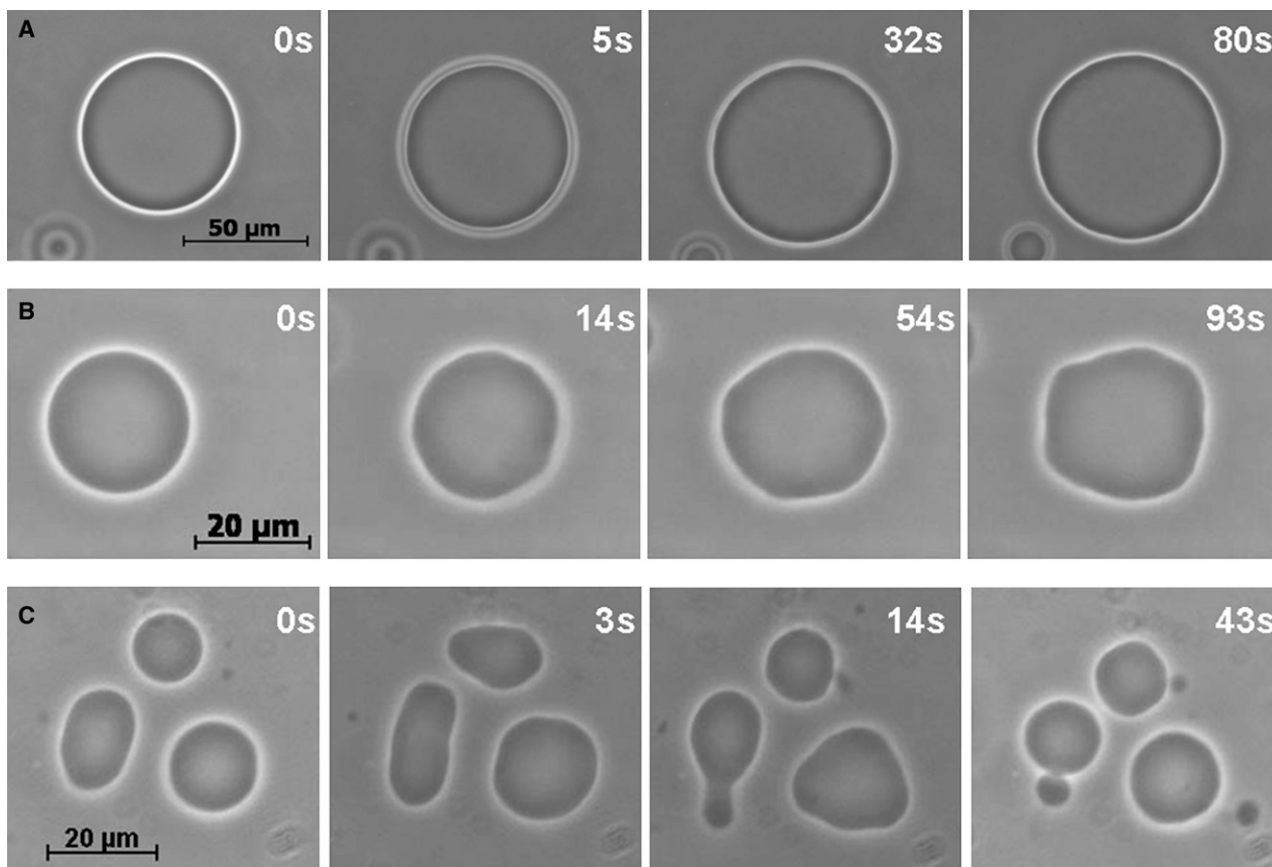
FIGURE 2   Effect of irradiation of POPC vesicles containing $X_{porph} = 0.02$ (A) and 0.05 (B and C). The irradiation time is shown on the top of each snapshot.

expulsion of buds, are due to a mechanism of vesicle surface area increase at constant volume.

The shape of a vesicle at equilibrium is defined from the minimization of the bending elastic energy of the lipid bilayer at constant area and enclosed volume, depending basically on two parameters: the area-to-volume ratio and the effective differential area between the two monolayers (14). Thus, any increase in area at constant volume modifies the area-to-volume ratio, inducing a change in the vesicle shape. A cartoon showing a side view of the main morphological changes induced by irradiation of GUVs is shown in Fig. 3. After irradiation, spherical vesicles gained excess area and became oblates (Fig. 3 B). Further increase in area caused one (Fig. 3 C) or many buds in a pearl chain (Fig. 3 D) to be expelled, to release the excess area.

The morphological changes observed in our experiments occurred only during the first seconds of irradiation, after which the vesicles did not show any significant evolution. Furthermore, the shape changes appeared irreversible, and vesicles did not show any alteration after the irradiation was stopped. In a previous work (16), GUVs destruction was observed after several minutes of irradiation, depending on the concentration of another photosensitive molecule, methylene blue, dispersed in the aqueous solution. Although both photosensitizers have practically the same singlet

oxygen production efficiency (Φ_Δ ~0.5), photosensitization in the presence of methylene blue appears to be more destructive when compared to the same $^1O_2$ flux produced by PE-porph (16). This is explained by the fact that, contrary to methylene blue, porphyrins are photooxidized during exposure to light (see Fig. 1 C). In fact, similar morphological changes associated with the increase in area were observed in the beginning of irradiation with methylene blue as described in Caetano et al. (16) and confirmed by us (results not shown), showing that increase in surface area is a trait of the initial steps of the oxidative damage, and is not caused by any specific effect of PE-porph. Another possible explanation for the differences in efficiency of GUV destruction between methylene blue and PE-porph may be the fact that methylene blue is also involved in dye-dye photosensitization processes, which may facilitate the progress of the peroxidation reactions (23,24).

Mechanisms of area increase

We showed in the previous section that irradiation of PE-porph incorporated in the bilayer induces morphological changes in giant vesicles, driven by an increase in surface area. When pure vesicles (in the absence of PE-porph) were irradiated, no significant effects were observed,
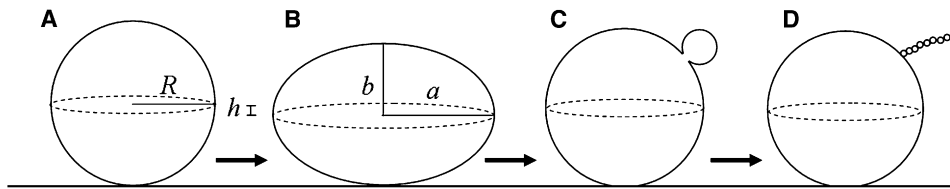
FIGURE 3 Schematic representation of the side view of the main morphological changes observed in vesicles as a result of irradiation of PE-porph: (*A*) initially spherical vesicle, (*B*) oblate vesicle, (*C*) expelling of one bud, and (*D*) expelling of various buds (pearl chain). The line below represents the coverslip.

although in few cases a small increase in area occurred, caused probably by the strong UV illumination. This increase was smaller than the increase observed for the lowest molar fraction of PE-porph incorporated in this study ($X_{porph} = 0.005$). Photoinduced morphological changes occurred only when PE-porph was present in vesicles made of unsaturated lipids, like POPC. For example, irradiation of PE-porph incorporated in GUVs made of DMPC, a saturated lipid, did not induce any relevant shape changes of the vesicles (results not shown). Thus, the observed area increase is associated to general oxidative reactions of the lipid double-bonds. It is also worth mentioning that hardly any area increase was detected when GUVs containing conventional fluorescent probes were irradiated. A previous work reported some side effects of production of oxygen reactive species by such probes, widely used in fluorescence microscopy of GUVs (25). This oxidative side effect caused by irradiation of fluorescent probes is, however, minute compared to the extensive oxidative damage caused by porphyrin. This can be explained because the main relaxation from the excited state in these probes occurs via fluorescent emission and not by intersystem crossing to the triplet state, as is the case for photosensitive molecules.

To test whether $^1O_2$ production was linked to the area increase, we performed irradiation of GUVs with $X_{porph} = 0.05$ in the presence of 1 mM sodium azide (NaN$_3$), a known $^1O_2$ quencher. In that situation, almost no morphological changes were observed, as can be seen in the example shown in Fig. 4. We can thus conclude that the general reaction of $^1O_2$ with lipid double-bonds is the main agent that causes
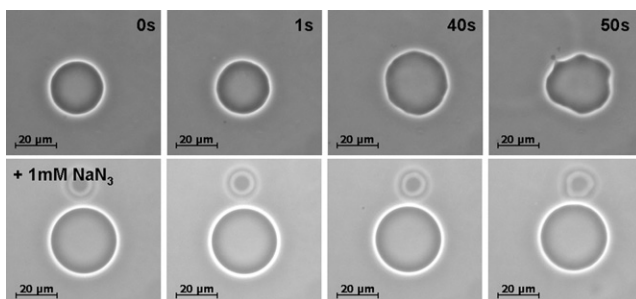
area increase. Lipid hydroperoxide is known to be the first stable product of this reaction (26), and it is thus reasonable to associate the observed area increase with the formation of hydroperoxides. This will be addressed later in Discussion.

Area increase measurement

Spherical vesicles changed initially into oblate-shaped vesicles as a result of irradiation; see cartoon in Fig. 3 *B*. Such deformation could, in principle, be used to roughly estimate the increase in surface area involved. However, because one of the semiaxes defining the oblate shape lies perpendicular to the focal plane, it cannot be directly assessed. Furthermore, deflated vesicles 1), might deform due to the contact with the coverslip; and 2), have some excess area hidden in fluctuations. Therefore, a different approach to estimate the area increase was used. It is known that in the presence of an AC field, lipid vesicles assume oblate or prolate shapes, with their symmetry axis lying parallel to the electric field, depending on the field frequency and conductivity ratio between the inner and outer solution (17). Thus, both semiaxes can be directly measured. In the case of oblate deformation, one of the long semiaxes lies perpendicular to the coverslip, thus susceptible to considerable deformations due to gravity. On the other hand, when the deformation is toward a prolate shape, one of the small semiaxes is perpendicular to the coverslip. Therefore, we chose to work with prolate shapes, because this implies less deformation due to the contact with the coverslip. For these experiments, vesicles containing $X_{porph} = 0.005-0.1$ were grown with a small quantity of salt and then diluted into a salt-free solution, so that the conductivity of the inner solution was higher. Under these conditions, AC fields always induce prolate deformations, irrespective of the field frequency (17). The irradiation was then performed in the presence of an AC field, and the increase in excess area was assessed from the increase in the degree of deformation. For a given field strength/frequency, the degree of deformation depends on the vesicle excess area. It is important to mention that the deformation induced by the weak AC field (10 V) is not enough to stretch the bilayer at the molecular level, as in the case of strong electric pulses (27) and pipette aspiration in the high tension regime (28). Instead, the deformation induced by the weak AC fields applied here acts only on the excess area, similar to experiments of aspiration with pipettes performed in the low tension regime (28).

FIGURE 4 Effect of sodium azide (NaN$_3$) on GUVs made of POPC containing $X_{porph} = 0.05$. The sequence shown on top was obtained in the absence of sodium azide, and clear morphological changes are observed as a result of irradiation. The sequence at the bottom was obtained in the presence of 1 mM NaN$_3$, and almost no changes are detected.
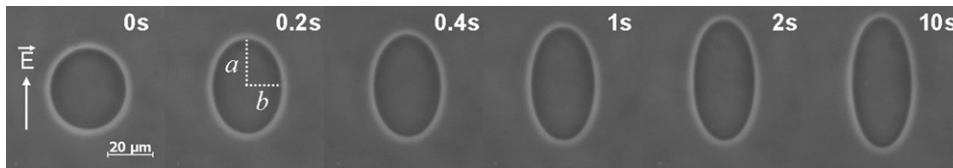
FIGURE 5 Irradiation of a GUV containing $X_{porph} = 0.03$ in the presence of an AC field (10 V, 1 MHz), which induces prolate deformation. The electric field direction is indicated on the left and the irradiation time on top of each snapshot. The scale bar represents 20 μm.

We chose vesicles that were initially almost spherical, i.e., had almost no excess area. Fig. 5 shows one example of irradiation of a GUV in the presence of an AC field. When the irradiation starts, the vesicle elongates as expected, assuming a prolate shape with its axis of symmetry lying parallel to the field, i.e., to the focal plane. From such sequence of images, the time evolution of both semiaxes was extracted. Each of these quantities shows a well-defined time variation: the largest semiaxis increases whereas the smallest semiaxis decreases with time.

Assuming that the vesicle shape is a prolate ellipsoid, both vesicle volume and surface area can be calculated. It should be noted that vesicles are not perfect prolates, as gravity and attractive interactions between the membrane and the substrate deform somewhat the vesicle. Within experimental error, the vesicle volume was roughly constant along the irradiation process (dispersion of $\pm 5\%$, not shown), whereas the surface area clearly increased with irradiation time.

Fig. 6 shows typical curves of the increase in area as a function of irradiation time for three GUVs ($X_{porph} = 0.01$, 0.05, and 0.1), as computed from the semiaxes of the prolate deformation in the presence of an AC field. The
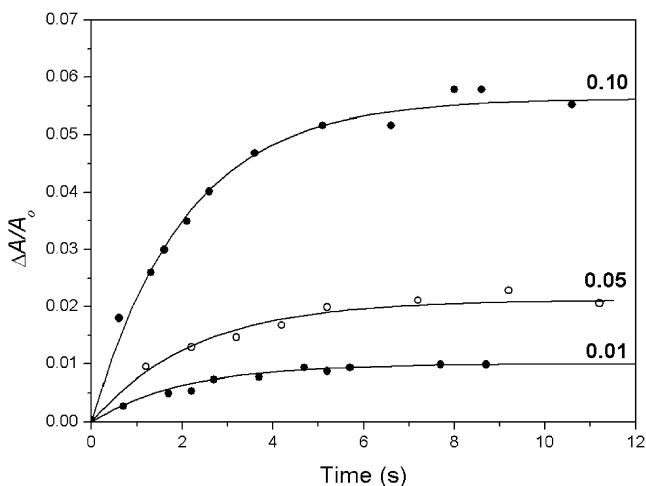
results show that the relative area expansion, $\Delta A/A_o$ (where A_o is the initial vesicle apparent surface area), varies exponentially as a function of time, reaching a maximum value, $\Delta A_{max}/A_o$ after a few seconds of irradiation. According to this behavior, one can assume that the relative increase in area is modulated by the PE-porph photobleaching that increases exponentially with a characteristic time τ, in such a way that

$$\frac{\Delta A}{A_o} = \frac{\Delta A_{max}}{A_o}\left(1 - e^{-t/\tau}\right). \tag{1}$$

The lines in Fig. 6 correspond to the best fittings to the experimental data according to Eq. 1. Fig. 7, A and B,

FIGURE 6 Relative area increase $(\Delta A/A_o)$ as a function of irradiation time of POPC GUVs containing $X_{porph} = 0.01$, 0.05, and 0.10, as indicated in the figure. The relative area increase was measured assuming prolate shape deformation of the GUVs in the presence of an AC field (see example in Fig. 5). The error in measuring the vesicle semiaxes is typically of the order of one pixel (~1%, since the typical vesicle diameter is ~100 pixels). This error was systematically smaller than the overall time evolution of the semiaxes lengths. The relative area increase was measured assuming that vesicles assume a prolate shape. We estimate the error of the relative area variation to be <10%.
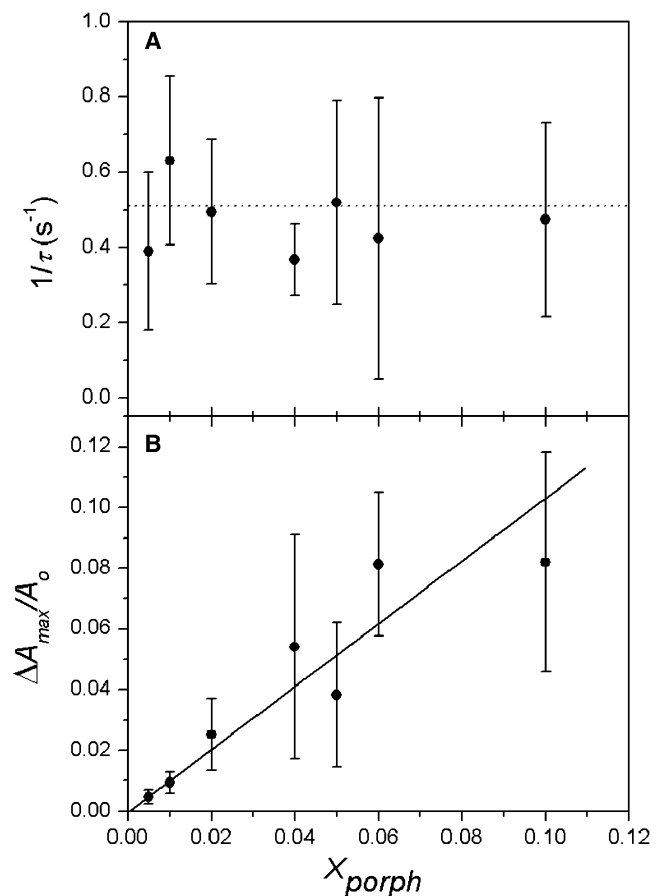

FIGURE 7 (A) Inverse of the characteristic time $(1/\tau)$ and (B) maximum relative area increase $(\Delta A_{max}/A_0)$ obtained from the fits to the data using Eq. 1 as a function of the PE-porph molar fraction in the membrane X_{porph}. The error bars represent measurements performed on different GUVs. At least five vesicles were used for each value of X_{porph}.

show the values of $1/\tau$ and $\Delta A_{\max}/A_0$, respectively, obtained as a function of X_{porph}. As one can see, the characteristic time is practically constant ($1/\tau = 0.51 \pm 0.13 \text{ s}^{-1}$), whereas $\Delta A_{\max}/A_0$ varies linearly with X_{porph} up to $X_{\text{porph}} = 0.10$. Furthermore, a photobleaching time of $\tau = 2$ s describes well the photobleaching observed under the conditions of our experiments (Fig. 1 C).

DISCUSSION

Our results clearly show that irradiation of photosensitive molecules close to lipid membranes of unsaturated lipids cause an increase in the bilayer surface area, which drives morphological changes of closed objects such as vesicles. We also show that the area increase is mainly driven by the reaction between singlet oxygen $^{1}O_2$ and lipid double-bonds, which is known to primarily produce lipid hydroperoxides LOOH (21). The hydroperoxide group has a more hydrophilic character compared to the lipid acyl-chain milieu. It is accepted that this group migrates to the bilayer surface (2,5,29), as schematically shown in Fig. 8. The lipid with the hydroperoxide group occupies a larger area (5,7–9), which seems to be the origin of the overall increase in bilayer
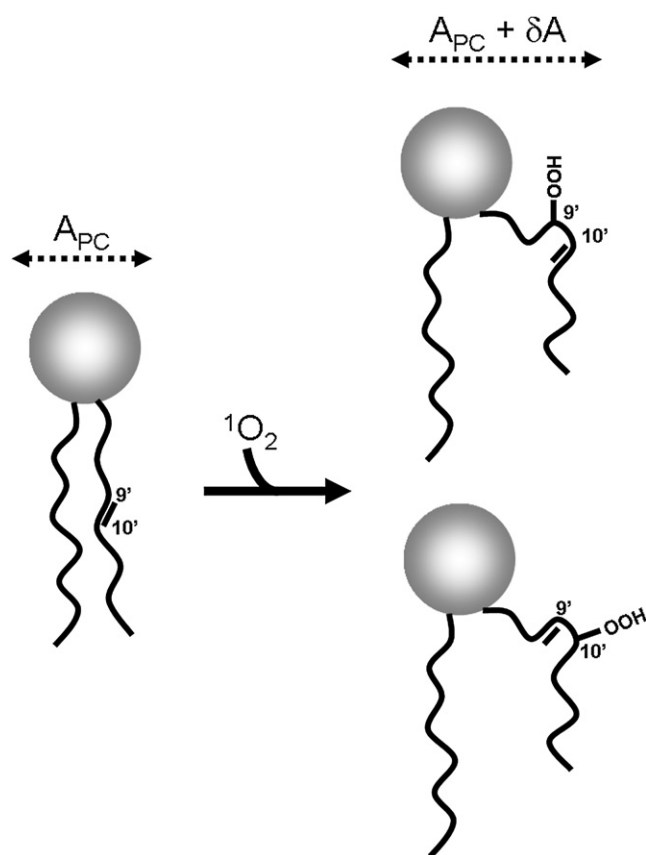

FIGURE 8 Schematic representation of the mechanism of area increase at the bilayer level. Singlet oxygen adds the more hydrophilic group -OOH at either 9′ or 10′ position, which migrates to the bilayer surface, imposing a kink to the acyl chain, with an accompanying increase in area δA per lipid.

surface area. If the oxidative reaction proceeds further, chain break can occur, producing an additional short-chain amphiphile, as observed previously after long time irradiation with methylene blue (16). However, since the reaction caused by irradiation of PE-porph is active only during the first seconds, due to photobleaching of the porphyrin group, we believe that the oxidative reaction is halted in its first step—namely, production of stable lipid hydroperoxides, which occupy a larger area per lipid, and induce the morphological changes observed in the GUVs.

There is no trivial way of directly quantifying the LOOH production in a single giant vesicle. Comparisons with LOOH production in small vesicles dispersion are not straightforward, as the experimental conditions are very different in both situations. In our setup, the irradiation is extremely intense and localized in the observation field, whereas in vesicle dispersions irradiation is not focused. However, we can assume that each LOOH produced adds a small increment (δA) to the total bilayer area. In a recently published work, Wong-ekkabut et al. (5) estimated the amount of area increase caused by formation of lipid hydroperoxides, using molecular dynamics simulations. A linear increase in the average area per lipid was obtained from simulations with bilayers containing up to 50 mol % of a lipid with a hydroperoxide group located at the ninth carbon of the acyl chain. Extrapolation of the data shown in Wong-ekkabut et al. (5) to 100 mol % LOOH shows that the area of one lipid may increase from 65 to 75 Å^2 with the formation of the hydroperoxide ($\delta A/A_{\text{PC}} \sim 0.15$). Using such an area increase per lipid, we can estimate the amount of hydroperoxides associated with the area increase experimentally observed in this work and subsequently determine a relation between the rate of $^{1}O_2$ production by PE-porph and the associated LOOH generation.

According to Busch et al. (30), the rate of $^{1}O_2$ production Q per photosensitive molecule is given by

$$Q = \frac{\Phi_\Delta \, \lambda P \sigma}{hc}, \qquad (2)$$

where Φ_Δ is the quantum yield of $^{1}O_2$ production of the photosensitive molecule, λ is the wavelength of the irradiation light (400 nm), P is the power density (see Materials and Methods), σ is the cross section of absorbance, h is the Planck's constant, and c is the speed of light. For porphyrin, $\Phi_\Delta = 0.5$ and σ (400 nm) $= 1.7$ Å^2. Thus, in our setup, PE-porph generates 900 $^{1}O_2$/s. Since PE-porph is anchored to the bilayer, we can assume that all $^{1}O_2$ produced will eventually hit the membrane. This is reasonable to assume, since the average diffusion range of $^{1}O_2$ in aqueous medium is around 100 nm (10).

By considering that the relative area increase, $\Delta A/A_o$, is directly related to the molar fraction of POPC molecules that transform into hydroperoxides, X_{LOOH}, we can write $\Delta A/A_o$ as

$$\frac{\Delta A}{A_\mathrm{o}} = \frac{X_\mathrm{LOOH}\ \delta A}{(1 - X_\mathrm{porph})A_\mathrm{PC} + X_\mathrm{porph}A_\mathrm{porph}}, \qquad (3)$$

where A_PC and A_porph are the areas of POPC ($65\ \text{Å}^2$) and PE-porph ($120\ \text{Å}^2$), respectively, and δA is the area increment due to peroxidation of one lipid ($\delta A = A_\mathrm{LOOH} - A_\mathrm{PC}$; $\delta A/A_\mathrm{PC} = 0.15$) (5). X_LOOH thus depends on the irradiation time and the efficiency n of the reaction between singlet oxygen and the phospholipids. In the absence of photobleaching, X_LOOH should linearly increase with time as

$$X_\mathrm{LOOH}(t) = n\,QX_\mathrm{porph}\ t. \qquad (4)$$

However, in the presence of photobleaching (see Fig. 1 C), the production rate of X_LOOH reads

$$X_\mathrm{LOOH}(t) = n\,Q\,X_\mathrm{porph} \int_0^t dt'\, e^{-t'/\tau}, \qquad (5)$$

where τ is the photobleaching time. Solving Eq. 5 and inserting the result in Eq. 3, we obtain

$$\frac{\Delta A}{A_\mathrm{o}}(t) = nQ\tau\,\frac{\delta A}{A_\mathrm{PC}}\,\frac{X_\mathrm{porph}A_\mathrm{PC}}{(1 - X_\mathrm{porph})A_\mathrm{PC} + X_\mathrm{porph}A_\mathrm{porph}}\left(1 - e^{-t/\tau}\right). \qquad (6)$$

Taking into account that X_porph is a small number compared to the molar fraction of POPC ($X_\mathrm{porph} \ll 1$), Eq. 6 can be approximated by

$$\frac{\Delta A}{A_\mathrm{o}}(t) = n\,Q\tau\,\frac{\delta A}{A_\mathrm{PC}}X_\mathrm{porph}\left(1 - e^{-t/\tau}\right). \qquad (7)$$

Comparing Eq. 7 to Eq. 1, one can obtain a relationship between $\Delta A_\mathrm{max}/A_\mathrm{o}$ and X_porph:

$$\frac{\Delta A_\mathrm{max}}{A_\mathrm{o}} = n\,Q\tau\,\frac{\delta A}{A_\mathrm{PC}}\ X_\mathrm{porph}. \qquad (8)$$

According to Fig. 7 B, $\Delta A_\mathrm{max}/A_0$ is described as a linear function of X_porph, with a slope close to 1. Since we know Q, τ, and the area increment $\delta A/A_\mathrm{PC}$, we can then calculate the efficiency n of the lipid peroxidation process via singlet oxygen: $n = 1/270$. This means that, on average, for each 270 singlet oxygen molecules reaching the membrane, one will interact chemically with the double-bound of the PC acyl chain and generate one lipid hydroperoxide. To our knowledge, this is the first time the efficiency of the reaction between phospholipids and singlet oxygen is evaluated in lipid bilayers. This relatively low value of $n \sim 0.0037$ is compatible with the low value of the total rate of suppression (chemical and physical) of $^1\mathrm{O}_2$ by phospholipids ($k_\mathrm{T} \sim 5 \times 10^4\ \mathrm{M}^{-1}\,\mathrm{s}^{-1}$) (31) and the value of n estimated for the oxidation of electron-rich olefin tetraphenylethylene by $^1\mathrm{O}_2$ ($n \sim 0.002$) in methanol solutions (32).

It is also interesting to analyze the number of LOOH molecules that are produced. According to Fig. 7 B, $\Delta A_\mathrm{max}/A_\mathrm{o}$

increases from 0.005 to 0.08 for $X_\mathrm{porph} = 0.005$–0.1. Using Eq. 3, we can associate this area increase with the peroxidation of 3–60% of the lipids. As we have already mentioned, the membrane remained intact under our experimental conditions, as can be seen by the permanence of the initial sugar asymmetry. Furthermore, no detectable change in vesicle volume was observed and no indication of macrodomain formation was detected. The bilayer surface seems to remain homogeneous. This result suggests that the membrane structure and plasticity may have a biological role in cell membranes in avoiding immediate rupture due to peroxidation, so that enzymatic defense has time to repair the phospholipids (33).

While studying the rupture of biological membranes of melanoma cells, Thorpe et al. (34) observed that the rupture initially occurred at single points in the plasma membrane. This effect was later modeled by Busch et al. (30) considering only the lipid part of the membrane and the effect of domain formation on the initial membrane rupture. Although some of the qualitative aspects of phenomena revealed by the numerical simulations of Busch et al. were also present in our experiments, i.e., the relationship between damage and $^1\mathrm{O}_2$ generation, the quantitative aspects reported here are markedly different. In particular, Busch et al. tested efficiency values n ranging from 0.2 to 0.03, i.e., at least 10 times above the values calculated from our experimental data. Thus, we show in this study that a high fraction of LOOH groups can be formed in the membrane even in the low n range. In addition, our results demonstrate that such high hydroperoxide content does not destroy the bilayer integrity, and does not lead to lipid domain formation or pore opening.

CONCLUSIONS

In this work we have studied a new photosensitive molecule, a porphyrin chemically linked to a lipid headgroup. When incorporated in lipid membranes, the photosensitive group resides at the bilayer surface. Thus, production of singlet oxygen occurs close to its main target, the double bonds of unsaturated lipids. This new photosensitizer allows for more controlled studies on the effect of lipid peroxidation.

We have studied the oxidative stress caused by the irradiation of this photosensitizer when incorporated in bilayers of unsaturated lipids forming GUVs, which can be observed with an optical microscope. Our results clearly show that lipid peroxidation causes an increase in bilayer area, which we measure as a function of the molar fraction of the photosensitive molecule incorporated and irradiation time. This is the first study to directly measure photoinduced area increase in lipid bilayers, which was previously observed experimentally only in monolayers (7–9). We associate the area increase with the production of hydroperoxides, which are known to occupy a larger area than normal unsaturated lipids, because of conformational changes imposed by migration of the more hydrophilic group to the bilayer surface (2,5,29). Strikingly,

peroxidation of as much as 60% of the lipids was still compatible with intact membranes. Using the rate of singlet oxygen production of the photosensitive molecule, we could estimate the efficiency of the oxidative process to be 0.0037. We expect that our results will help in the development of improved models of membrane photoinduced damage, which may be of help in the fields of photodynamic therapy as well as of UV-A induced skin damage.

REFERENCES

1. Schnitzer, E., I. Pinchuk, and D. Lichtenberg. 2007. Peroxidation of liposomal lipids. *Eur. Biophys. J.* 36:499–515.

2. van Ginkel, G., J. H. Muller, F. Siemsen, A. A. van't Veld, L. J. Korstanje, et al. 1992. Impact of oxidized lipids and antioxidants, such as vitamin E and lazaroids, on the structure and dynamics of unsaturated membranes. *J. Chem. Soc., Faraday Trans.* 88:1901–1912.

3. Megli, F. M., and K. Sabatini. 2003. Respiration state IV-generated ROS destroy the mitochondrial bilayer packing order in vitro. An EPR study. *FEBS Lett.* 550:185–189.

4. Jacob, R. F., and R. P. Mason. 2005. Lipid peroxidation induces cholesterol domain formation in model membranes. *J. Biol. Chem.* 280:39380–39387.

5. Wong-ekkabut, J., Z. Xu, W. Triampo, I.-M. Tang, D. P. Tieleman, et al. 2007. Effect of lipid peroxidation on the properties of lipid bilayers: a molecular dynamics study. *Biophys. J.* 93:4225–4236.

6. Sotto-Arriaza, M. A., C. P. Sotomayor, and E. A. Lissi. 2008. Relationship between lipid peroxidation and rigidity in L-α-phosphatidylcholine-DPPC vesicles. *J. Colloid Interface Sci.* 323:70–74.

7. Abousalham, A., F. Fotiadu, G. Buono, and R. Verger. 2000. Surface properties of unsaturated non-oxidized and oxidized free fatty acids spread as monomolecular films at an argon:water interface. *Chem. Phys. Lipids.* 104:93–99.

8. Abousalham, A., and R. Verger. 2006. Continuous measurement of the lipoxygenase-catalyzed oxidation of unsaturated lipids using the monomolecular film technique. *Pharmacol. Res.* 23:2469–2474.

9. Sabatini, K., J.-P. Mattila, F. M. Megli, and P. K. J. Kinnunen. 2006. Characterization of two oxidatively modified phospholipids in mixed monolayers with DPPC. *Biophys. J.* 90:4488–4499.

10. Ochsner, M. 1997. Photophysical and photobiological processes in the photodynamic therapy of tumors. *J. Photochem. Photobiol. B Biol.* 39:1–18.

11. Valenzeno, D. P. 1987. Photomodification of biological membranes with emphasis on singlet oxygen mechanisms. *Photochem. Photobiol.* 46:147–160.

12. Engelmann, F. M., I. Mayer, D. Gabrielli, K. Araki, H. E. Toma, et al. 2007. Interactions of cationic *meso*-porphyrins with biomembranes. *J. Bioenerg. Biomembr.* 39:175–185.

13. Tarr, M., A. Frolov, and D. P. Valenzeno. 2001. Photosensitization-induced calcium overload in cardiac cells: direct link to membrane permeabilization and calcium influx. *Photochem. Photobiol.* 73:418–424.

14. Döbereiner, H.-G. 2000. Properties of giant vesicles. *Curr. Opin. Colloid Interface Sci.* 5:2560263.

15. Dimova, R., S. Aranda, N. Bezlyepkina, V. Nikolov, K. A. Riske, et al. 2006. A practical guide to giant vesicles. Probing the membrane nanoregime via optical microscopy. *J. Phys. Condens. Matter.* 18:S1151–S1176.

16. Caetano, W., P. S. Haddad, R. Itri, D. Severino, V. C. Vieira, et al. 2007. Photo-induced destruction of giant vesicles in methylene blue solutions. *Langmuir.* 23:1307–1314.

17. Aranda, S., K. A. Riske, R. Lipowsky, and R. Dimova. 2008. Morphological transitions of vesicles induced by alternating electric fields. *Biophys. J.* 95:L19–L21.

18. Angelova, M. I., and D. S. Dimitrov. 1986. Liposome electroformation. *Faraday Discuss. Chem. Soc.* 81:303–311.

19. Uchoa, A. F., P. P. Knox, N. K. Seifullina, and M. S. Baptista. 2008. Singlet oxygen generation in the reaction centers of *Rhodobacter sphaeroides*. *Eur. Biophys. J.* 37:843–850.

20. Tanielian, C., and G. Heinrich. 1995. Effect of aggregation on the hematoporphyrin-sensitized production of singlet molecular oxygen. *Photochem. Photobiol.* 61:131–135.

21. Brault, D., C. Vever-Bizet, and T. L. Doan. 1986. Spectrofluorimetric study of porphyrin incorporation into membrane models—evidence for pH effects. *Biochim. Biophys. Acta.* 857:238–250.

22. van Steveninck, J., J. W. M. Lagerberg, P. Charlesworth, T. M. A. R. Dubbelman, and T. G. Truscott. 1994. Effects of the micro-environment on the photophysical properties of hematoporphyrin. *Biochim. Biophys. Acta.* 1201:23–28.

23. Severino, D., H. C. Junqueira, D. S. Gabrielli, M. Gugliotti, and M. S. Baptista. 2003. Influence of negatively charged interfaces on the ground and excited state properties of methylene blue. *Photochem. Photobiol.* 77:459–468.

24. Junqueira, H. C., D. Severino, L. G. Dias, M. Gugliotti, and M. S. Baptista. 2002. Modulation of the methylene blue photochemical properties based on the adsorption at aqueous micelle interfaces. *Phys. Chem. Chem. Phys.* 4:2320–2328.

25. Ayuyan, A. G., and F. S. Cohen. 2006. Lipid peroxides promote large rafts: effects of excitation of probes in fluorescence microscopy and electrochemical reactions during vesicle formation. *Biophys. J.* 91:2172–2183.

26. Girotti, A. W. 2001. Photosensitized oxidation of membrane lipids: reaction pathways, cytotoxic effects, and cytoprotective mechanisms. *J. Photochem. Photobiol. B Biol.* 63:103–113.

27. Riske, K. A., and R. Dimova. 2005. Electro-deformation and -poration of giant vesicles viewed with high temporal resolution. *Biophys. J.* 88:1143–1155.

28. Evans, E., and W. Rawicz. 1990. Entropy-driven tension and bending elasticity in condensed-fluid membranes. *Phys. Rev. Lett.* 17:2094–2097.

29. Buettner, G. R. 1993. The pecking order of free radicals and antioxidants: lipid peroxidation, α-tocopherol, and ascorbate. *Arch. Biochem. Biophys.* 300:535–543.

30. Busch, N. A., M. L. Yarmush, and M. Toner. 1998. A theoretical formalism for aggregation of peroxidized lipids and plasma membrane stability during photolysis. *Biophys. J.* 75:2956–2970.

31. Krasnovsky, Jr., A. A., and V. E. Kagan. 1979. Photosensitization and quenching of singlet oxygen by pigments and lipids of photoreceptor cells of the retina. *FEBS Lett.* 108:152–154.

32. Machado, A. E. H., M. L. Andrade, and D. J. Severino. 1995. Oxidation of an electron-rich olefin induced by singlet oxygen: mechanism for tetraphenylethylene. *Photochem. Photobiol. A Chem.* 91:179–185.

33. Girotti, A. W. 1998. Lipid hydroperoxide generation, turnover, and effector action in biological systems. *J. Lipid Res.* 39:1529–1542.

34. Thorpe, W. P., M. Toner, R. M. Ezzell, R. G. Tompkins, and M. L. Yarmush. 1995. Dynamics of photoinduced cell plasma membrane injury. *Biophys. J.* 68:2198–2206.